JOURNAL OF SPACECRAFT AND ROCKETS
Vol. 32, No. 3, May–June 1995

Predicting Thermal Contact Resistance at Cryogenic Temperatures for Spacecraft Applications

J. Maddren* and E. Marschall†
University of California, Santa Barbara, Santa Barbara, California 93106

Extensive work has been done to predict thermal contact resistance (or thermal contact conductance) at room temperature; however only limited research has been conducted at cryogenic temperatures. The absence of experimental data is notable because of the many applications for spacecraft at low temperature. This paper presents thermal contact conductance measurements of pressed metal contacts in a vacuum environment near room temperature and at cryogenic temperatures (110 to 144 K). Contact pressures varied from 0.4 to 14 MPa. The materials used were chosen because of their applications within the aerospace industry: stainless steel (AISI 304), aluminum (6061-T6), a low-expansion nickel–iron alloy (39% nickel), and beryllium. Existing theoretical correlations (an elastic contact model and a plastic contact model) are reviewed, and the temperature dependence of the relevant material properties is investigated to explain the results. The stainless-steel data are in good agreement with the elastic contact model, whereas the aluminum data do not agree well with either the elastic or the plastic contact model. Of particular interest are the results with beryllium that indicate the conductance may not always be directly proportional to the bulk thermal conductivity.

Nomenclature

A_a = actual contact area, m^2
A_n = nominal contact area, m^2
D_s = density of summits, m^{-2}
d = mean summit plane separation, m
E = Young's modulus, N/m^2
E' = equivalent Young's modulus, $[((1-\nu_1^2)/E_1)+((1-\nu_2^2)/E_2)]^{-1}$, N/m^2
F_n = functions for the Greenwood–Williamson model
H = hardness, kg/mm^2
h_c = thermal contact conductance, W/m^2 K
k = thermal conductivity, W/m K
m = mean absolute profile slope, $(m_1^2+m_2^2)^{\frac{1}{2}}$
n = contact spot density, m^{-2}
P = nominal contact pressure, N/m^2
R = mean summit radius, m
Rq = RMS roughness σ, m
s = variable of integration
T = mean interface temperature, K
t = dimensionless mean summit plane separation d/σ_s
x = dimensionless mean plane separation, $Y/\sqrt{2}\sigma$
Y = mean plane separation, m
ν = Poisson's ratio
σ = standard deviation of the profile height distribution, $(\sigma_1^2+\sigma_2^2)^{\frac{1}{2}}$, m
σ_s = standard deviation of summit height distribution, m
ψ = contact resistance factor

Introduction

MANY spacecraft electronic components, such as focal-plane detector arrays used in satellite imaging systems, operate efficiently only at low temperatures within narrow limits. Prediction of operating temperatures requires correct modeling of the heat path from source to sink. A primary factor limiting heat transfer is the thermal contact resistance across metal contacts such as bolted joints. Therefore, proper modeling of metal interfaces at cryogenic temperatures is necessary.

For applications involving cooling of electronics across bolted joints, the parts will be assembled at room temperature. If the deformation of the contacting asperities is elastic, then the problem of contact mechanics and heat transfer should be solved at the operating temperature. If the deformation is plastic and the hardness increases with decreasing temperature, then there will be no further plastic deformation upon cooling down to the operating temperature (assuming the joint is subjected to a uniform pressure independent of temperature). Therefore, the problem will involve solving the contact mechanics at room temperature and solving the heat transfer problem at cryogenic temperatures. In order to successfully model thermal contact resistance, it is first necessary to understand how the contact mechanics and heat transfer depend upon temperature.

An extensive literature search was conducted; however, only two experimental studies of thermal contact resistance in the temperature range from liquid nitrogen to room temperature were found.[1,2] Comparison of the data of these studies with available correlations was inconclusive.[1,2] Fletcher and Gyorog[3] noted that attempts by another researcher to correlate the contact conductance data of Ref. 1 over a wide range of temperatures indicated that the mean interface temperature exerts a stronger effect on the contact conductance than can be accounted for by the temperature dependence of the material properties. No explanation was given for this result.

This paper presents thermal contact conductance measurements for a variety of materials over the range of temperatures from liquid nitrogen to room temperature. Existing theoretical correlations are reviewed, and the temperature dependence of the relevant material properties is investigated to explain the results.

Theory

Elastic Contact

The modified Greenwood–Williamson elastic contact model[4] is fairly easy to use and has been shown to yield accurate results.[4,5] A brief review of the equations will be given here. For a more detailed treatment of the derivation the reader is referred to Refs. 5 and 6.

The model considers elastic contact between a plane and a nominally flat surface covered with a large number of spherical asperities. The summit density is assumed to be uniform over the rough surface. It is further assumed that all the asperities have the same radius and their height vary randomly. The contact spot density, the ther-

Presented as Paper 93-2775 at the AIAA 28th Thermophysics Conference, Orlando, FL, July 6–9, 1993; received July 8, 1993; revision received Dec. 27, 1993; accepted for publication Dec. 27, 1993.

*Research Assistant, Department of Mechanical and Environmental Engineering. Student Member AIAA.
†Professor, Department of Mechanical and Environmental Engineering.

mal contact conductance, the actual contact area, and the nominal pressure are given by

$$n = D_s F_0(t) \tag{1}$$

$$h_c = 2\psi^{-1} k D_s R^{\frac{1}{2}} \sigma_s^{\frac{1}{2}} F_{\frac{1}{2}}(t) \tag{2}$$

$$A_a = \pi A_n D_s R \sigma_s F_1(t) \tag{3}$$

$$P = \tfrac{4}{3} E' D_s R^{\frac{1}{2}} \sigma_s^{\frac{3}{2}} F_{\frac{3}{2}}(t) \tag{4}$$

The contact resistance factor can be approximated by the following relation[7]:

$$\psi \approx \left[1 - (A_a/A_n)^{\frac{1}{2}}\right]^{\frac{3}{2}} \tag{5}$$

If the summit heights are assumed to follow a Gaussian distribution, then

$$F_n(t) = \frac{1}{\sqrt{2\pi}} \int_t^\infty (s-t)^n e^{-\frac{1}{2}s^2}\, ds \tag{6}$$

where values of the function for $n = 0, \frac{1}{2}, 1, \frac{3}{2}$ have been tabulated.[8] The summit density, the asperity radius, and the standard deviation of the summit height distribution can be evaluated from profile measurements of the surface.[4,5]

Plastic Contact

Yovanovich[9] reviewed the relevant equations for plastic contact. Yovanovich and Hegazy[10] have reported excellent agreement between the model and experimental data. The actual contact area, the contact spot density, and the thermal contact conductance are given by

$$\frac{A_a}{A_n} = \frac{P}{H} = \frac{1}{2}\operatorname{erfc}(x) \tag{7}$$

$$n = \frac{1}{16}\left(\frac{m}{\sigma}\right)^2 \frac{\exp(-2x^2)}{\operatorname{erfc}(x)} \tag{8}$$

$$h_c = \frac{1}{2\sqrt{2\pi}} k\psi^{-1}\left(\frac{m}{\sigma}\right)\exp(-x^2) \tag{9}$$

The expression for the conductance can be approximated by the following relation[9]:

$$h_c = 1.25k\left(\frac{m}{\sigma}\right)\left(\frac{P}{H}\right)^{0.95} \tag{10}$$

for $2 < Y/\sigma < 4.75$.

What are the relevant material properties in each model, and what is their temperature dependence? First, the surface topography is assumed to be independent of temperature. Note the following:

1) Both the elastic and plastic contact models predict that the conductance is directly proportional to the thermal conductivity.

2) The plastic model predicts that the conductance is very nearly inversely proportional to the hardness.

3) The elastic model predicts that the conductance is very nearly inversely proportional to the equivalent Young's modulus.

For the materials considered in this study, the change in the elastic constants over the temperature ranges considered was always less than 10%. For this reason their influence will be largely ignored.

Experimental Apparatus

All specimens of the same material were machined from the same rod. The specimens measured 2.54 cm in diameter and 3.81 cm in length. The contacting surface of each specimen was ground flat. Some of the specimens were then bead blasted to produce a rough, isotropic surface. A summary of the surface preparation for each experiment is listed in Table 1. All experiments involved contact between specimens of the same material with nominally similar surface texture. Surface profiles of the specimens were measured with a Dektak 8000 stylus profilometer. The sampling interval was approximately 2.5 μm with a total trace length of 5.0 mm. The profile output of height as a function of sample was recorded for later evaluation.

Table 1 Summary of experiments

Expt.	Material	Surface texture	R_q, μm	T, K	k, W/m K
1	Stainless steel	Bead blasted	2.20	326	15.0
2	Stainless steel	Bead blasted	2.16	110	10.0
3	Aluminum	Bead blasted	5.62	355	188
4	Aluminum	Bead blasted	5.83	131	158
5	Nickel–iron	Ground	0.47	292	15.7
				144	12.7
6	Nickel–iron	Ground	0.41	294	15.7
				125	12.1
7	Beryllium	Ground	0.60	293	210
				116	410

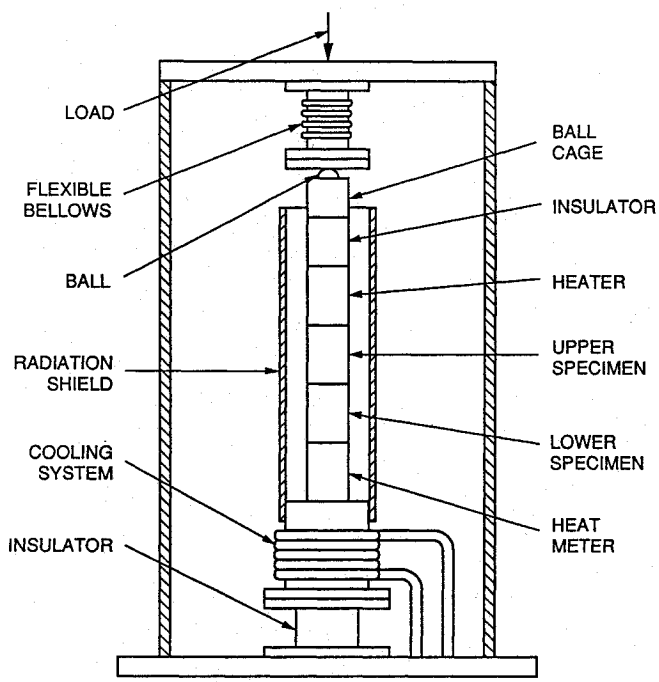

Fig. 1 Experimental apparatus.

The experimental apparatus is shown in Fig. 1. All experiments were conducted in a vacuum environment (less than 5×10^{-4} torr) near room temperature or below. Therefore heat transfer across the interface was limited to conduction through the contacting asperities. The load was applied by a lever arm through a flexible bellows at the top of the chamber. The linearity and lever ratio of the loading were verified by a load cell outside the chamber. Thermal insulators were used above the heater and below the cooling coil to thermally isolate the test column from the environment. The heater consisted of a cartridge heater epoxied into a copper cylinder. The heat was removed at the base of the column through a copper cooling coil. For room-temperature experiments, the cooling fluid used was a water–glycol mixture, and for the cryogenic experiments liquid nitrogen was vaporized through the cooling coil. The heat flow through the test column was adjusted to give a measurable temperature drop across the interface at the highest loads and also maintain a mean interface temperature close to the sink temperature. The heat flow through the column was measured by a heat meter situated between the lower specimen and the cooling coil. Two separate heat meters were used, which were close to the thermal conductivity of the specimens: austenitic stainless steel for the experiments with stainless steel and the nickel–iron alloy, and electrolytic iron for the experiments with aluminum and beryllium. Temperatures in the specimens and heat meter were measured at four locations along the axis of symmetry. Thermocouples (type E, 36 gauge) were inserted into ra-

dial holes drilled 5 mm deep and 0.64 mm in diameter and secured with a silver epoxy. The thermal conductivity of the specimens could be determined from the measured temperature gradients in the heat meter and the specimens, assuming a constant heat flow through the column. A passive radiation shield to prevent radial heat losses from the column was attached to the base and was maintained near the sink temperature.

Experimental Procedure

The specimens were initially brought into contact at room temperature. A contact pressure of approximately 0.1 MPa was applied to the specimens, and then the chamber was evacuated. The vacuum was maintained for at least 24 h before taking any measurements. The load was incremented approximately 1 MPa for both the loading and unloading stages. Steady state was assumed when the measured temperature change in the specimens and the heat meter was less than 0.1 K over a 10-min interval.

Experimental Uncertainty

The error in the measured conductance was evaluated using the methods outlined by Birge[11] with a probability of 10:1. The error was a function of load because of the decreasing measured temperature jump across the interface with increasing load. The range of experimental uncertainty in the measured conductance for each experiment is listed in Ref. 12. The experimental uncertainty in the measured thermal conductivity was always less than 5%.

All experiments were conducted in a vacuum environment at pressures less than 5×10^{-4} torr. However, the specimens were assembled prior to evacuating the chamber, and thus some air could have been trapped between the two contacting surfaces. An independent experiment was conducted at very low contact pressure to estimate the thermal contact conductance due to conduction through the interstitial media (air). At low contact pressures the conductance due to solid–solid contact will approach zero while the conductance due to conduction through the interstitial media will remain constant. At a nominal contact pressure of 8.7 kPa, the total conductance was measured to be 52 W/m^2 K. The contribution due to solid–solid conduction was estimated to be 12 W/m^2 K by measuring the conductance at higher contact pressures (almost entirely due to solid–solid contact) and extrapolating the data to 8.7 kPa. Therefore, after neglecting heat transfer due to radiation, the conductance due to conduction through the interstitial media was estimated to be 40 W/m^2 K (independent of the material properties of the contacting solids and the gap thickness). This represents a maximum error of 8% for the experiment with stainless steel at room temperature at the lowest load. For higher-conductivity materials (aluminum and beryllium) and/or at higher loads the conductance due to solid–solid contact will be greater and the error will be significantly less.

Results

Figures 2 and 3 show the results of two separate experiments with stainless steel (AISI 304) specimens; one experiment was conducted above room temperature ($T = 326$ K), and one at a cryogenic temperature ($T = 110$ K). Both specimen pairs were bead blasted and possessed nominally similar roughness (see Table 1). The results show two complete load cycles as indicated in each figure. Both experiments show little difference in conductance between the first loading and the subsequent unloading. These results indicate the deformation during the first load cycle is predominantly elastic. Also note that the conductance does not increase during the second load cycle in comparison with the first load cycle. Therefore, the deformation is almost completely elastic after the first loading. The elastic model agrees well with the data from both experiments. The decrease in the conductance from the experiment at 326 K to the experiment at 110 K is equal to the decrease in thermal conductivity associated with the decrease in mean interface temperature. This result is exactly what the elastic model predicts. Figure 4 shows the hardness variation as a function of temperature for stainless steel (AISI 304) and aluminum (6061-T6).[13] The hardness was measured using a diamond pyramid indenter; specific information concerning the load used in the tests was not available. As shown in Fig. 4,

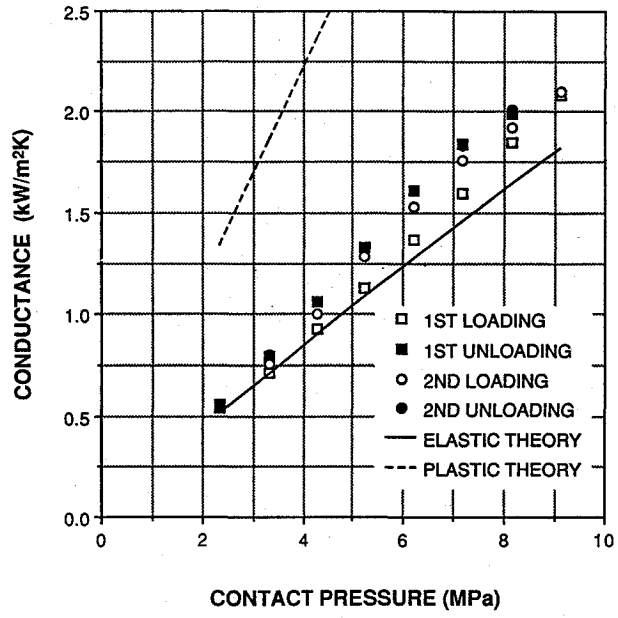

Fig. 2 Contact conductance vs nominal contact pressure for stainless steel (AISI 304) (experiment 1: $T = 326$ K, $k = 15.0$ W/m K).

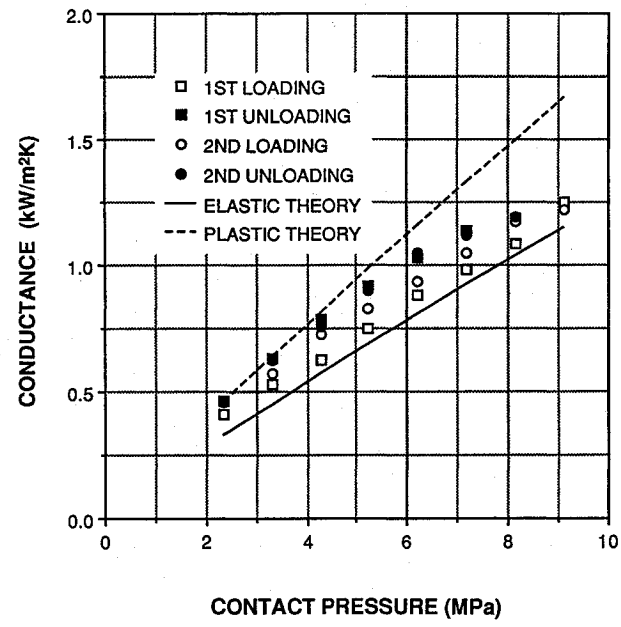

Fig. 3 Contact conductance vs nominal contact pressure for stainless steel (experiment 2: $T = 110$ K, $k = 10.0$ W/m K).

the hardness of the stainless steel increases over 60% for the temperature decrease from 326 to 110 K. There is not a corresponding decrease in the measured conductance. It must be concluded that the deformation is elastic and that use of a plastic contact model to predict thermal contact conductance at cryogenic temperatures can result in large errors.

Figures 5 and 6 show similar results with aluminum (6061-T6) specimens. One experiment was conducted above room temperature ($T = 355$ K), and one at a cryogenic temperature ($T = 131$ K). Both specimen pairs were bead blasted and possessed nominally similar roughness (see Table 1). Both experiments show a notable increase in the conductance from the first loading to the first unloading, which indicates there is some plastic deformation. However, the conductance does not increase during the second load cycle in comparison with the first load cycle. Therefore the deformation is almost completely elastic after the first loading. The decrease in the measured conductance (approximately 50%) from the experiment

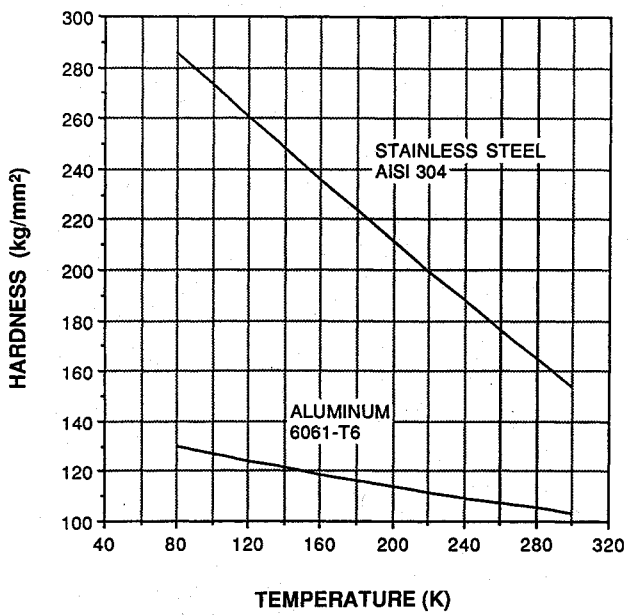

Fig. 4 Hardness vs temperature for stainless steel (AISI 304) and aluminum (6061-T6).

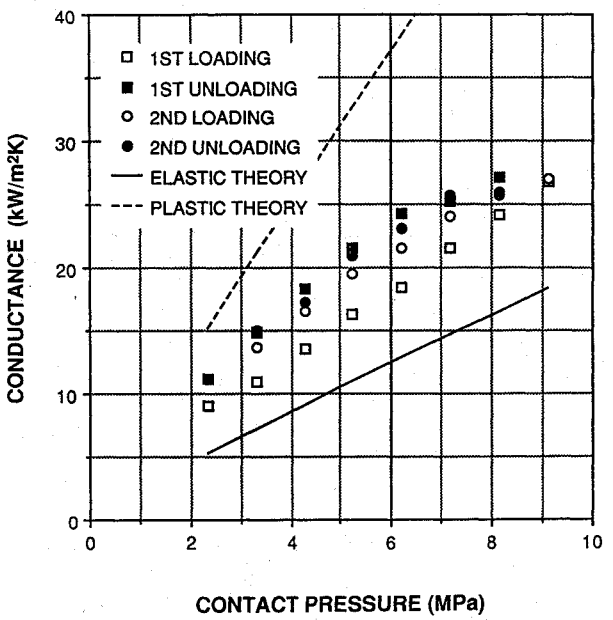

Fig. 6 Contact conductance vs nominal contact pressure for aluminum (experiment 4: $T = 131$ K, $k = 158$ W/m K).

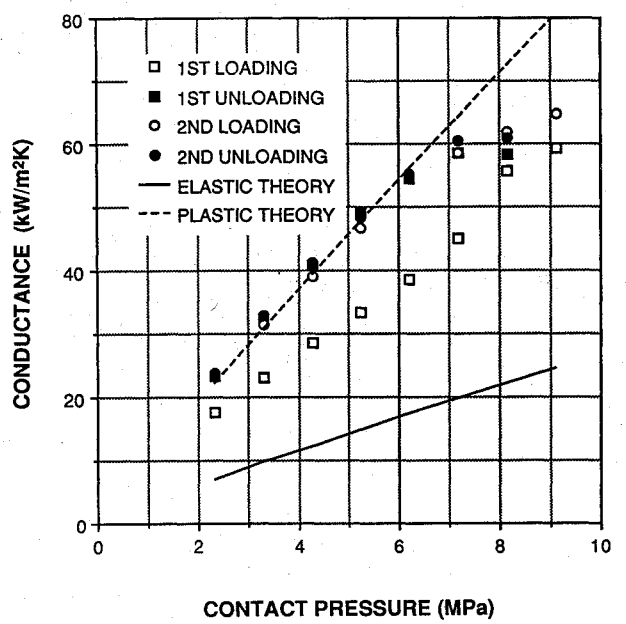

Fig. 5 Contact conductance vs nominal contact pressure for aluminum (experiment 3: $T = 355$ K, $k = 188$ W/m K).

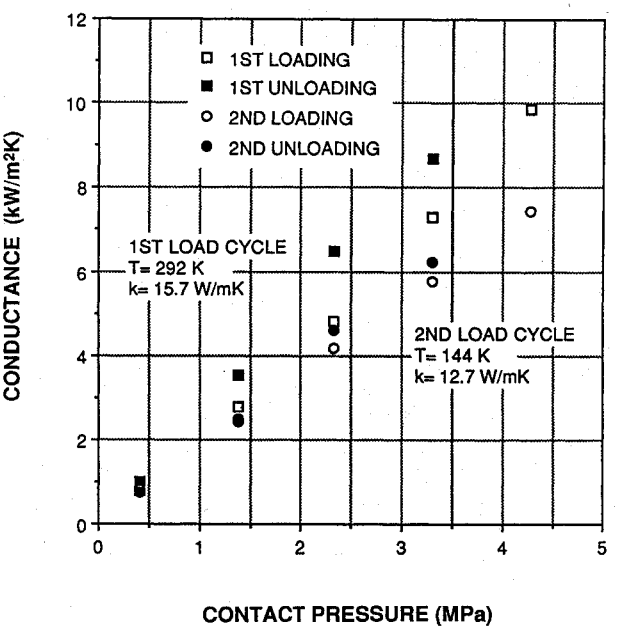

Fig. 7 Contact conductance vs nominal contact pressure for nickel–iron alloy (experiment 5).

at 355 K to the experiment at 131 K is larger than the decrease in the thermal conductivity (16%). As shown in Fig. 4, the hardness increases over 20% for the same temperature change. This would support the conclusion that the predominant mode of deformation is plastic; however, agreement between the data and the plastic contact model is poor.

These experiments show the differences between the contact conductance for materials deformed near room temperature and at cryogenic temperatures. For spacecraft applications at low temperature involving conductance across bolted joints, the parts will be assembled at room temperature. When the spacecraft is in orbit, the component will be cooled to the operating temperature. Since the hardness increases with decreasing temperature for most materials, the conductance across the bolted joint will be larger than shown for an experiment where the interface was loaded at cryogenic temperatures if the predominant mode of deformation is plastic. To successfully model the application, the following experimental procedure was proposed: measure the conductance for one complete load cycle at room temperature, and then cool the specimens and measure the conductance for another load cycle at low temperature.

Figure 7 shows the results of an experiment with a low-expansion nickel–iron alloy (39% nickel). The first load cycle was conducted at room temperature ($T = 292$ K), and the second at a cryogenic temperature ($T = 144$ K). After the first load cycle was completed, the specimens were then cooled at the lowest load. The specimens were not separated, and the vacuum was not interrupted between the first load cycle and the second load cycle. After the specimens were cooled and steady state was achieved, the second load cycle was commenced. There appears to have been some permanent deformation in the first load cycle, as indicated by the hysteresis. There also appears to be little plastic deformation on the second load cycle. To compare the changes in conductance between the first and second load cycles, the difference should be measured between the first unloading and the second unloading. The experimental results show that the decrease in the conductance was slightly larger than the

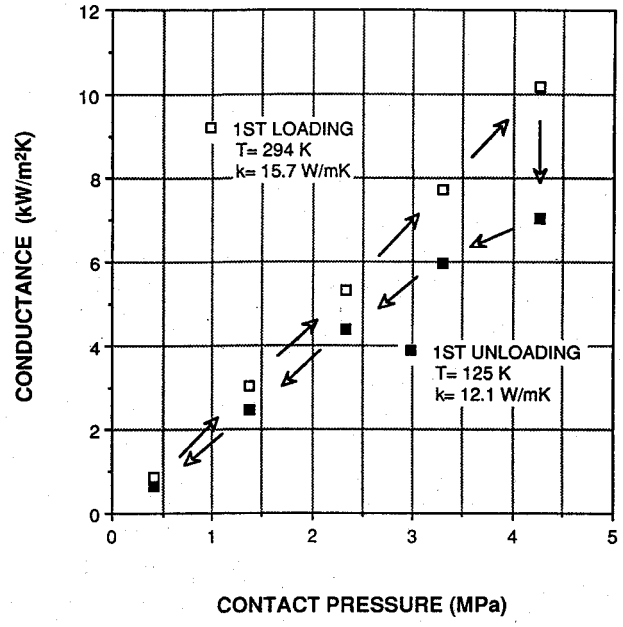

Fig. 8 Contact conductance vs nominal contact pressure for nickel–iron alloy (experiment 6).

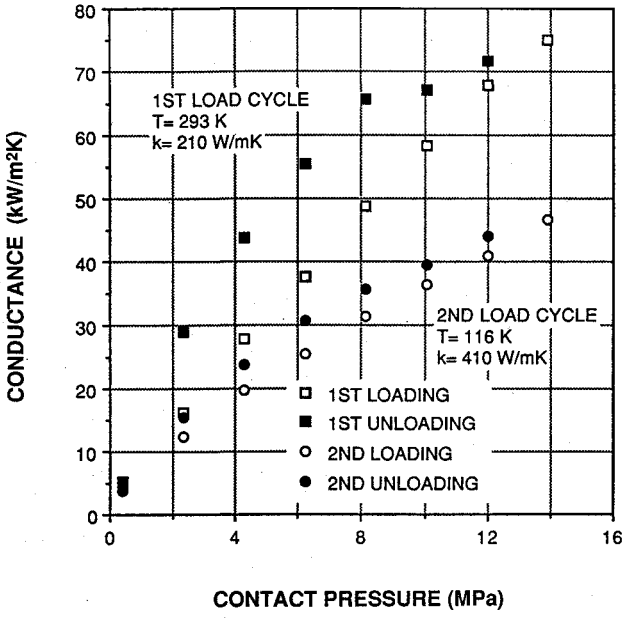

Fig. 9 Contact conductance vs nominal contact pressure for beryllium (experiment 7).

decrease in the thermal conductivity. The decrease in the conductance was approximately 25–30%, and the decrease in the thermal conductivity was 19%.

The experiment described above is not exactly the same as the procedure followed in an application. Rather, the above procedure was undertaken to be able to compare the changes in conductance over the range of pressures. To verify the applicability of the experimental results presented in Fig. 7, a similar experiment was conducted using the low-expansion alloy. In this experiment, the conductance was measured at room temperature ($T = 294$ K) up to the highest load and then cooled to a cryogenic temperature ($T = 125$ K) without unloading. The decrease in the measured conductance was 31% and the decrease in the thermal conductivity was 23%. The results are shown in Fig. 8. This experiment supports the applicability of the procedure outlined previously to measure the change in conductance due to a change in temperature over a range of pressures. Both of the experiments with the nickel–iron alloy indicate the thermal contact conductance is nearly directly proportional to the thermal conductivity.

Another experiment was conducted using beryllium, which is of interest to the aerospace industry on account of its extremely high strength-to-weight ratio. Figure 9 shows the results of the experiment with beryllium. The first load cycle was conducted at room temperature ($T = 293$ K). The specimens were then cooled at the lowest load, similarly to the experiment with the nickel–iron alloy, and then the second load cycle was conducted at cryogenic temperature ($T = 116$ K). The large hysteresis in the first load cycle indicates there was some permanent deformation; however, there is only a small hysteresis in the second load cycle, indicating that the deformation is mostly elastic. The contact conductance decreased by approximately 45% over the entire load cycle, whereas the measured thermal conductivity increased by 95%. It is obvious that the use of available correlations to extrapolate the contact conductance measured at room temperature to predict the conductance at cryogenic temperatures would lead to large errors.

The beryllium used in the previously described experiment was vacuum hot-pressed. Its chemical composition was low in beryllium oxide, with a minimum of 99% beryllium. This was the only material in the study with very high purity. All the other materials were alloys with larger concentrations of impurities.

For a fairly pure metal almost the entire observed thermal conductivity is due to the electrons. At sufficiently low temperatures, theory predicts the thermal conductivity will vary linearly with temperature because of scattering caused by static imperfections. At higher temperatures scattering due to phonons becomes more important. If the thermal resistivity due to static imperfections grows comparably to the resistivity due to phonon scattering at sufficiently low temperatures, then the thermal conductivity $k(T)$ passes through a maximum and decreases at higher temperatures. However, in alloys and metals of high defect concentration, scattering due to imperfections and to phonons become comparable only at higher temperatures; in such cases there is no maximum, but the thermal conductivity only increases monotonically as a function of temperature.[14] At this time, we can only infer the cause of the phenomenon observed in the experiment with beryllium, but it is postulated that the bulk thermal conductivity is not an accurate measure of the thermal conductivity at or near the interface, because of the presence of more static imperfections than in the bulk material.

Conclusions

The present study measured the thermal contact conductance across pressed metal contacts in a vacuum environment near room temperature and at cryogenic temperatures. The experiments with stainless steel exhibited predominantly elastic deformation (small hysteresis in the first load cycle) and were in good agreement with the elastic contact model. The experiments with aluminum displayed some degree of plastic deformation (larger hysteresis in the first load cycle) but did not agree well with the elastic or plastic contact models.

The experiments with the nickel–iron alloy (39% Ni) and beryllium were conducted specifically for the purpose of modeling thermal contact resistance for spacecraft applications where the parts are assembled at room temperature and then cooled down to the operating temperature of the component. The thermal contact conductance was measured for one complete load cycle at room temperature, and then the specimens were cooled and the conductance was measured for another complete load cycle at cryogenic temperatures. Some hysteresis was noted in the first load cycle; the hysteresis in the second load cycle was significantly less, indicating that the contact area was already established during the first load cycle. The experiments with the nickel–iron alloy indicated that the thermal contact conductance is nearly directly proportional to the thermal conductivity. This observation supports both the elastic and the plastic contact models. Surprisingly, however, the experiments with beryllium exhibited anomalous behavior. It was noted for one experiment that upon cooling to cryogenic temperatures the contact conductance decreased by approximately 45% over the range of contact pressures, whereas the measured thermal conductivity increased by 95%. At this time the cause of the phenomenon can only be inferred, but it is postulated that the bulk thermal conductivity is not an accurate measure of the thermal conductivity at or near

the interface, because of the presence of more static imperfections than in the bulk material.

The different phenomena observed in the experiments for this small sampling of materials and surface textures indicate that there is still much to learn about thermal contact conductance at cryogenic temperatures. Of particular interest are the results with beryllium, and further work must be conducted to ascertain the cause of the anomalous behavior.

Acknowledgments

This work was supported by the Santa Barbara Research Center and the State of California through a MICRO grant. The authors would also like to thank Sloan Technology of Santa Barbara and Fujitsu Computer Packaging Technologies of San Jose for profile measurements of the surfaces.

References

[1]Bloom, M. F., "Thermal Contact Conductance in a Vacuum Environment at Low Temperatures," *Proceedings of the 4th Conference on Thermal Conductivity*, U.S. Naval Radiological Defense Lab., 1964, pp. III-F-1–III-F-34.

[2]Thomas, T. R., and Probert, S. D., "Thermal Contact Resistance: The Directional Effect and Other Problems," *International Journal of Heat and Mass Transfer*, Vol. 13, May 1970, pp. 789–807.

[3]Fletcher, L. S., and Gyorog, D. A., "Prediction of Thermal Contact Conductance Between Similar Metal Surfaces," AIAA Paper 70-852, June 1970.

[4]McWaid, T. H., and Marschall, E., "Application of the Modified Greenwood and Williamson Contact Model for the Prediction of Thermal Contact Resistance," *Wear*, Vol. 152, Jan. 1992, pp. 263–277.

[5]McCool, J. I., "Comparison of Models for the Contact of Rough Surfaces," *Wear*, Vol. 107, Jan. 1986, pp. 37–60.

[6]Greenwood, J. A., and Williamson, J. B. P., "Contact of Nominally Flat Surfaces," *Proceedings of the Royal Society of London, Series A: Mathematical and Physical Sciences*, Vol. 295, Dec. 1966, pp. 300–319.

[7]Cooper, M. G., Mikic, B. B., and Yovanovich, M. M., "Thermal Contact Conductance," *International Journal of Heat and Mass Transfer*, Vol. 12, March 1969, pp. 279–300.

[8]Maddren, J., McWaid, T. H., and Marschall, E., "Thermal Contact Resistance of Pressed Metal Contacts at Cryogenic Temperatures," *29th National Heat Transfer Conference*, Aug. 1993.

[9]Yovanovich, M. M., "Thermal Contact Correlations," AIAA Paper 81-1164, June 1981.

[10]Yovanovich, M. M., and Hegazy, A., "Experimental Verification of Contact Conductance Models Based upon Distributed Surface Micro-hardness," AIAA Paper 83-0532, Jan. 1983.

[11]Birge, R. T., "The Calculation of Errors by the Method of Least Squares," *Physical Review*, Vol. 40, April 1932, pp. 207–227.

[12]Maddren, J., and Marschall, E., "Predicting Thermal Contact Resistance at Cryogenic Temperatures for Spacecraft Applications," AIAA Paper 93-2775, July 1993.

[13]Mann, D., *LNG Materials and Fluids*, 1st ed., National Bureau of Standards, Boulder, CO, 1977.

[14]Grigull, U., and Sandner, H., *Heat Conduction*, 1st ed., Hemisphere, Washington, DC, pp. 7–9.

M. E. Tauber
Associate Editor